International Journal of Adhesion & Adhesives 149 (2026) 104320

Contents lists available at ScienceDirect

International Journal of Adhesion and Adhesives

journal homepage: www.elsevier.com/locate/ijadhadh

Identifying the optimal flexural performance of metal-composite single-lap joints with copolyester-reinforced epoxy adhesive under various loading rates using the Grey Relation Analysis

Engin Erbayrak [a,*], Seda Erbayrak [a], Beril Eker [b], Murat Colak [c]

[a] Istanbul Gelisim University, Faculty of Engineering & Architecture, Istanbul, Turkey
[b] Yıldız Technical University, Rectorate, Istanbul, Turkey
[c] Bayburt University, Vocational School, Bayburt, Turkey

ARTICLE INFO

Keywords:
Metal-composite single-lap joints
6-Node pentahedral cohesive element
Grey relation analysis
Flexural test

ABSTRACT

This study examines the best flexural performance of metal composite single-lap joints fabricated with copolyester-reinforced epoxy adhesives at various loading rates using the Grey Relation Analysis (GRA). The study consists of three parts. The first part involves the formation of metal composite single-lap joints and their experimental approach under different loading rates. In the experimental approach, A356 aluminum was used as the metal material with the addition of titanium (Ti) and boron (B) additives. Plain-woven glass fiber-reinforced epoxy (GFRE) and plain-woven carbon fiber-reinforced epoxy (CFRE) were served as the composite materials. The lap joints were tested in three-point bending tests under loading rates of 1, 10, and 50 mm/min, respectively. In the second part, a numerical analysis was conducted using boundary conditions similar to the experimental conditions. In the numerical analysis, a 6-node pentahedral cohesive element was utilized, representing a novel approach for modeling adhesives in finite element analysis (FEA). When experimental and numerical results were compared, a difference of 4.36% was observed between the maximum load values and 6.80% between the failure displacements. Based on these results, it can be said that the experimental results converge with the numerical results. In the last part of the study, performance rankings of metal composite joints were determined using the Grey Relational Analysis (GRA) method, which enabled us to identify the optimum joint. This systematic approach facilitated the scientific design of joints that demonstrate optimal flexural performance under various loading conditions.

1. Introduction

Metal-composite lap joints are being widely used in various industries, especially in the aviation industry. In a metal-composite lap joint, the predominant metal is aluminum, and the composite components are mainly carbon-fiber and glass-fiber reinforced composite materials [1–3]. These lap joints are subjected to various loading conditions, which depend on their different applications. Among these, bending load is one of the main concerns. M. Rezvaninasab et al. [4] investigated the effects of pin and wire reinforcements on the flexural strength of aluminum-glass composite single-lap joints under bending loads. They tested four different configurations of the metal-composite single-lap joints at a bending rate of 0.5 mm/min. They concluded from their results that the pin reinforcement gave more flexural strength and toughness than that for wire reinforcement. Darla et al. fabricated a single-lap joint by using carbon fiber reinforced plastic (CFRP) and aluminum. They used a pre-coating treatment (RPC) and surface treatment with sodium hydroxide (NaOH) on the adherends of aluminum alloy. The primary aim of their research was to find the optimum contact angle for metal-composite joints with different surface treatments under a bending load. To determine this, they used the Young-Laplace measurement technique. They found from their results that the surface-treated metal-composite joints gave significantly better maximum bending strength than that of untreated joints [5]. E. Esmaeili et al. [6] conducted research on the influence of adding metal fibers to the adhesive in a metal-composite single-lap adhesive joint on the strength of the joint structure under a bending load. The study consisted of experimental and numerical analyses. They found that the addition of

* Corresponding author.
E-mail address: eerbayrak@gelisim.edu.tr (E. Erbayrak).

https://doi.org/10.1016/j.ijadhadh.2026.104320
Received 3 November 2025; Received in revised form 27 December 2025; Accepted 5 March 2026
Available online 6 March 2026

metal fibers to adhesives increased the flexural strength of the joint structure significantly. Results for the numerical analysis also agreed with the experimental results through the finite element approach. A. Zeinedini et al. [7] researched riveting as a technique for joining metal-composite single-lap joints. They tested riveted joints under a bending load, with Al 6061-T6 alloy as the metal in the lap joint and woven E-glass/epoxy composite as the composite part in that joint. The results from their experimental procedure were in good agreement with the results obtained from the finite element method. Furthermore, the experimental results showed that the energy absorption of the single lap joints was increased considerably by the embedding method. A. Sadık and F. Karabudak [8] carried out tensile and flexural tests on metal composite single-lap joints made using adhesives and bolts and also damage analyses. They used AZ91 Mg alloy as the metal and carbon fiber composite as the composite material. The adhesive used in their tests was a type of acrylic adhesive named Acryton 1E1. The tests, carried out at a constant loading rate, demonstrated that the flexural strength of the adhesive-made metal composite joint was higher than that of the bolted joint.

Numerical modeling of single-lap joint structures has been performed by many researchers. H. El-Etri et al. [9] conducted both experimental and numerical studies on the strength of single-strap lap joints subjected to flexural loads. In the numerical model, they modeled the adherends forming the lap joint using an 8-node brick solid element (C3D8R) and the cohesive region with an 8-node linear cohesive element (COH3D8). Besides, they used the trapezoidal cohesive zone method in order to model the adhesive. They presented that maximum bending load and related displacement values obtained from the numerical model were in good agreement with the results obtained from the experimental approach. GC Papanicolaou and coworkers investigated the strength of single-lap joints made from similar and dissimilar adherends under bending loads. They have investigated joint configurations at various wood, PVC, and titanium sheet adherends and tested seven different bond lengths such as 25, 30, 35, 40, 45, and 50 mm. To verify the experimental approach, they have proposed a numerical model by using the finite element method with consistent boundary conditions. The results of the numerical analysis showed that the joints made from different materials become stiffer when increasing the bond length. Besides, they verified that the numerical results were in good agreement with the experimental results [10]. F. Kadıoğlu and M. Demiral [11] conducted experimental and numerical studies on the performance of a single-lap joint made from composite laminates with various fiber orientations under flexural loading. The finite element model was prepared by using ABAQUS/Explicit software. To model the possible damage in the composite laminates after loading, the Hashin failure criterion was implemented. Their research results show that the fiber orientations of composite laminates have a big effect on the flexural performance of the lap joint. A. Azam et al. [12] conducted experimental and numerical studies on the behavior of T-joint composite lap joint under bending load. They investigated how the composite laminate with different orientations would affect the bending stiffness of a T-joint model. The T-joint lap joint was modeled by the researchers using a standard mesh structure with eight-node and six-node elements, specifically in the radius regions, while taking the hourglass effect into consideration in the finite element model. Their results indicated that the damage in the T-joint lap model under bending load originated at the points of stress concentration at the far ends of the adhesive layer, with the cracks propagating toward the center of the T-joint. Most importantly, they noted that the results derived from the finite element analysis agreed well with the experimental results.

There are several decision-making methods available in the literature for determining the optimal design of metal and composite materials under various loading conditions. Among these approaches, the GRA method is notably preferred since it can express the results obtained from pairwise comparisons of each criterion. This technique provides greater accuracy and reliability of the decision-making process. Lee et al. [13] identified the optimal design for a flexural mechanism of a work plate featuring a 12-inch hole at its center. They made use of grey relational analysis and orthogonal arrays specifically for the XYθ micro positioning stage. Besides this, they incorporated the optimization results with a finite element analysis. Their findings showed that the optimization results were in agreement with both the finite element study and experimental approaches. Ibrahim Sabry and colleagues [14] studied the mechanical properties of a flange made from 6061-T3 aluminum alloy joined by a friction stir weld. During welding, they established different levels for factors such as travel speed, rotation speed, and shoulder diameter. In order to optimize the process, they made use of the Grey Relational Analysis (GRA) multi-criteria decision-making method. Results from the GRA indicated that friction stir welding was an efficient method for the improvement of quality responses. Dixit and Jain [15] focused on the optimization of parameters such as extrusion temperature, layer thickness, and build direction in the manufacture of thermoplastic polyurethane (TPU) by Additive Manufacturing. In their study, they employed the Grey Relational Analysis (GRA) multi-decision analysis method. Their research indicated that GRA significantly optimized various process parameters associated with Fused Filament Fabrication (FFF) for the maximum strengthening of flexible parts printed. Besides that, the experimental results obtained using the GRA approach proved efficient for improving multi-reactivity of these flexible components. Hamid and Seyyed [16] conducted research into the joining of copper sheets through Friction Stir Welding (FSW), investigating 12 different process parameters including rotational speed, traverse speed, and shoulder surface diameter. The mechanical properties of the joint area were evaluated through tensile and shear tests. The authors used Grey Relational Analysis to optimize the welding parameters applied in this joining technique. The optimization results indicated that the optimal conditions related to obtaining the best mechanical properties included a shoulder surface diameter of 25 mm, a rotational speed of 1120 rpm, and a travel speed of 22 mm/min.

The present study investigated the optimal flexural performance of a metal composite lap joint made up of co-polyester-reinforced epoxy adhesive under different loading rates. Three-point bending tests at various loading rates were conducted to investigate the flexural performance of a lap joint. A 6-node pentahedral cohesive element, an innovative approach for modeling adhesives in finite element analyses, was used during numerical analysis. The experimental data were then verified by comparing the results with those coming from the FEM, thus confirming the reliability of our data. Eventually, the GRA technique was implemented in order to rank the performance of the metal composite joints and find the best configuration.

2. Experimental approach

2.1. Manufacturing of the metal-composite lap joint

In this section, the manufacturing of the single lap joint will be described first. The single lap joint is made from aluminum and composite adherends with a co-polyester-reinforced epoxy adhesive. The metal and composite materials used in this study are widely preferred engineering materials, especially in the aerospace industry. Additionally, the epoxy-based adhesives employed in the single lap joints are frequently discussed in the literature and are commonly used in similar applications. These materials were selected and assessed in this study because of their direct relevance to both industry applications and existing research.

Composite laminates used for this study were manufactured using the VARTM process. During the VARTM process, the mold surface was covered by sealing tapes; then a release film was positioned on the top. Dried layers of reinforcement were placed successively, followed by the introduction of a flow medium to achieve uniform delivery of resin and hardener. Spiral hoses attached to both the resin and vacuum pumps were responsible for air evacuation out of the vacuum bag and the intake

of the epoxy-hardener mixture. This operation was maintained until complete impregnation of the fibers took place. Afterwards, the layup was cured on a hot plate at 100 °C for 1 h. The composite laminates, manufactured in eight plies with warp/weft directions, were cut to the required dimensions for lap joints by means of a water jet as shown in Fig. 1 A.

The aluminum adherends were manufactured from scraps through the processes of melting and casting. Scraps of aluminum material are melted in a 10 kW electric resistance furnace; the resultant melted aluminum was then cast at a temperature of 720 °C, when the casting processes required that the melted aluminum be cast at that temperature. To ensure good processing of the aluminum alloy, titanium (Ti) and boron (B) were added to the molten aluminum in an amount equal to 0.01% of the total aluminum alloy content. One of the key processes in the casting technique was ensuring that the melted aluminum was pure. This was achieved through the use of a rotary degassing system. This system uses a specifically designed graphite lance that was immersed in the melted aluminum at a predetermined speed, which created a certain kind of whirl in the melted aluminum. The whirl created an opportunity for the introduction of nitrogen gas into the melted aluminum. As a result of the 300 rpm speed created by the impeller of the rotary systems coupled with a 5 L per minute rate of gas movement in the apparatus, the nitrogen gas formed bubbles in the melted aluminum that eliminated any gases present in the aluminum. The melted aluminum was then poured into sand molds. The purity of the melted aluminum was then analyzed using a Reduced Pressure Test (RPT) apparatus that involved applying a reduced air pressure to the aluminum that was hardening. The method used in the aluminum metal was successful in that it provided an opportunity for the gases that had not been eliminated in the aluminum metal to grow in the apparatus. The aluminum adherends manufactured in the casting processes were then removed from their casting molds. Aluminum adherends were then fitted with their measurements in a lap joint system in accordance with Fig. 1-B.

Araldite AV138M epoxy adhesive, supplied by Huntsman Corporation, was mixed with a high-hardness, heat-resistant co-polyester thermoplastic (Copes) manufactured by Schaetti® using a vacuum-assisted mixing system. The mechanical and physical properties of the adhesive and the thermoplastic have already been stated in the previous studies of

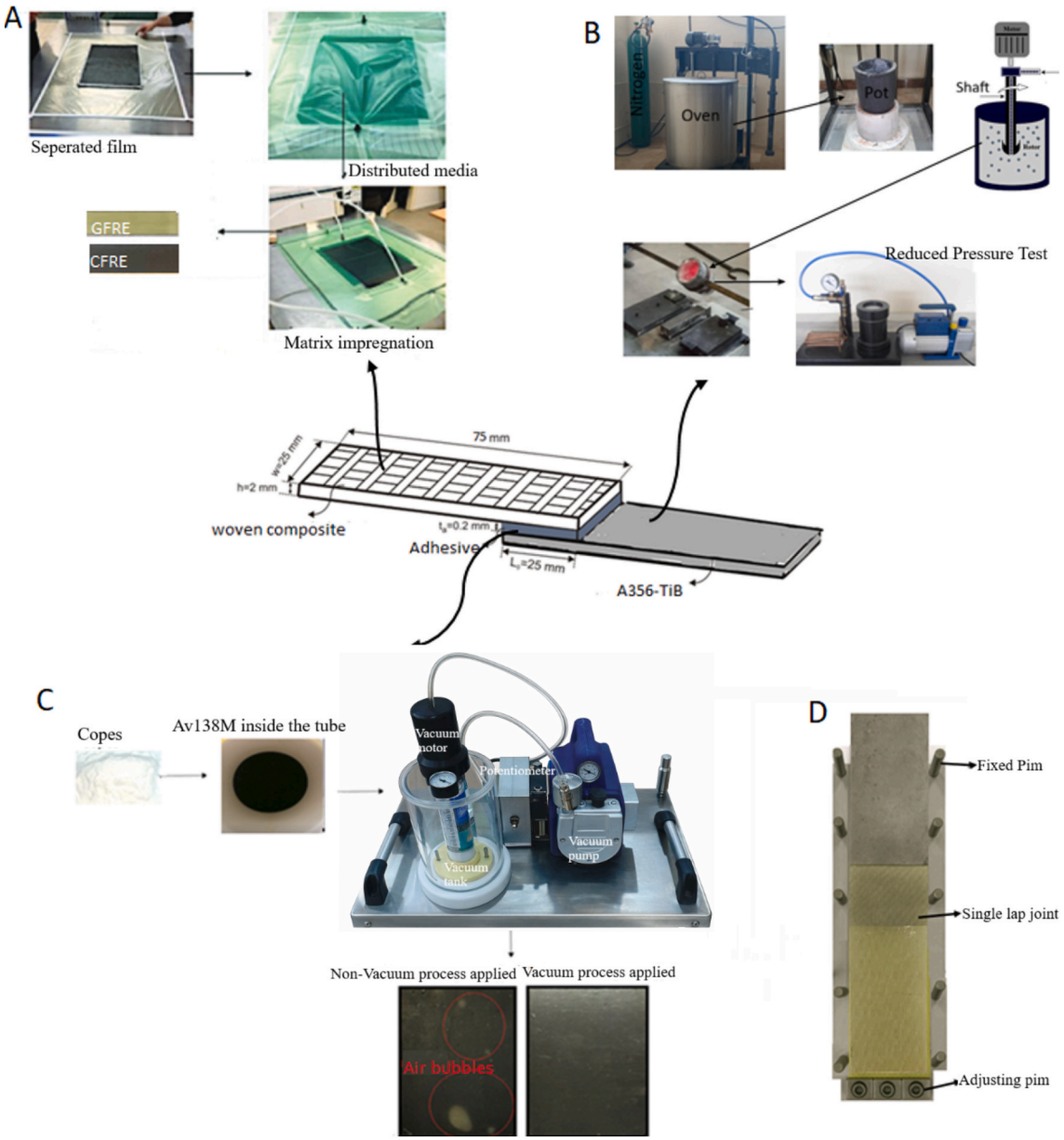

Fig. 1. Manufacturing steps for single lap joint (a) Casting process (b) VARTM (c) Vacuum mixing (d) Molding.

the authors [17,18]. In order to avoid the development of air bubbles, which can weaken the bond strength during the mixing of adhesives with hardeners and additives, the process was carried out under vacuum conditions. This method effectively eliminated air bubbles from the adhesives. The vacuum mixing device includes several key parts such as a vacuum chamber, a plastic container for storing adhesive, a DC motor, a mixing paddle, a potentiometer for the control of speed, a vacuum gauge, a filter, a control valve, and a vacuum pump. The pump has a capacity of 850 mbar, whereas a proper control valve located between the vacuum tank and the pump provides the possibility of accurately stabilizing the vacuum pressure inside the chamber at the desired level. The mixing speed inside the chamber is precisely controlled with the potentiometer in such a way that uniform mixing occurs under vacuum conditions, as presented in Fig. 1-C. In addition, the difference between the adhesive plate fabricated using vacuum mixing and the one without is demonstrated in the figure. Air bubbles are remarkably visible on the adhesive plate that was not created under vacuum conditions.

Single-lap joints were fabricated using a custom-designed mold. Fixed pins prevented any lateral displacement during curing, while adjusting pins allowed the fabrication of joints with different dimensions. The thickness of the adhesive layer in the mold was achieved by using 0.2 mm-thick Mylar tape. A mold release agent was used to ensure easy demolding. The curing process of the single lap joint placed in the mold was carried out by allowing it to cure at room temperature for 24 h. The full fabrication process of single-lap joints is shown in Fig. 1-D.

Four different single lap joints were prepared within the scope of the study. These are GFRE-Al-Av138M epoxy (GF-AL-138M), GFRE-Al-Copes reinforced Av138M (GF-AL-CO138M), CFRE-Al-Av138 M (CF-AL-138M), and CFRE-Al-Copes reinforced Av138M (CF-Al-CO138M). A total of 36 single-lap joints were tested at three different loading rates, with three samples of each bonded joint.

2.2. Determining the mechanical properties of the materials that formed the lap joint

The mechanical performance of A356 and A356–TiB alloys was evaluated through uniaxial tensile testing. All experiments were conducted using a universal testing machine that operated at a constant loading rate of 1 mm/min. For each alloy, three specimens were tested, and the mean values were calculated using the Moving Average method in MATLAB. The tensile specimens were fabricated in accordance with the ASTM E8 standard. The corresponding stress-strain responses for the A356 and A356–TiB alloys are illustrated in Fig. 2.

Fig. 2 demonstrates that the maximum tensile strength and strain of A356 aluminum significantly increase with the addition of TiB. It is noteworthy that no heat treatment was applied to the aluminum alloys utilized in this study. This choice was deliberate to effectively illustrate the impact of TiB addition on aluminum material sourced exclusively from scrap aluminum. It is well established that heat treatment can influence the mechanical properties of aluminum [19]. The mechanical properties of the aluminium alloys are given in Table 1.

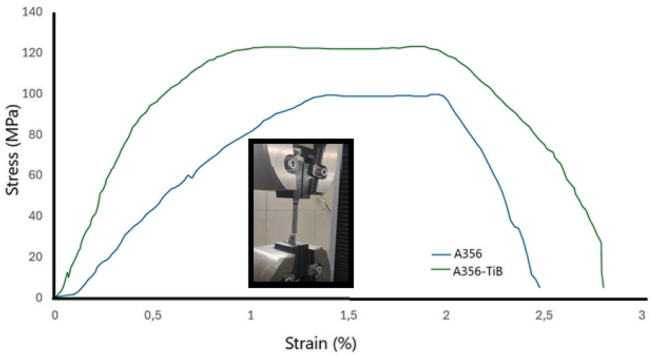

Fig. 2. The stress-strain curves of aluminum.

The thermoplastic copolyester (CoPES) was blended into the Araldite Av138M epoxy adhesive in varying proportions, with the most significant change in mechanical performance observed at a 20% addition level. Tensile specimens were created in accordance with BS 2782 standards and tests were carried out using a universal testing machine, with a loading rate of 1 mm/min. For each adhesive formulation, three individual samples were evaluated. The stress-strain responses for the unreinforced and reinforced adhesives are shown in Fig. 3.

As illustrated, adding copolyester to the epoxy system increased the strain, while the ultimate tensile strength decreased. This change suggests a shift toward more ductile behavior in the adhesive due to the presence of the thermoplastic additive. Furthermore, the mechanical properties of both the reinforced and unreinforced adhesives can be seen in Table 2.

Coupon tests were conducted by the authors on composite laminates used in lap joints, and their mechanical properties have been documented in the existing literature [20]. This phenomenon will not be discussed further here to maintain brevity.

2.3. Three-point flexural test

Flexural tests were performed using the INSTRON 5982 universal testing machine at room temperature. The single lap joints were prepared following the ASTM D790 standard. A span length of 60 mm was chosen, as it aligns with existing literature [21]. Three samples were tested for each single lap joint configuration, resulting in a total of 36 samples tested. The setup for the flexural tests is shown in Fig. 4.

In the flexural test, all single lap joint configurations were subjected to three different loading rates (1 mm/min, 10 mm/min, 50 mm/min). It should be stated here that determining the loading rates for the flexural test, we carefully considered the loading conditions that metal-composite lap joints encounter in real-world applications [22]. Recent experimental research on hybrid metal-composite adhesive joints indicates that dynamic loading conditions rates ranging from approximately 10^0 to 10^2 s^{-1} significantly influence both joint strength and energy absorption properties when compared to quasi-static loading conditions [23,24]. Consequently, the loading rates applied in this study were determined with consideration of the relevant literature. At the end of the flexural tests, load-displacement curves were obtained for each loading rate. The maximum load, displacement and flexural modulus values calculated from curves were read on the testing device's interface. Using load-displacement data obtained from the experimental approach, the stress, strain, and flexural modulus for the flexure are calculated as follows

$$\begin{aligned} \sigma &= \left(\frac{3F_{mid}L}{2wt^2}\right) \\ \varepsilon &= \left(\frac{6\delta t}{L^2}\right) \\ E &= \left(\frac{mL^3}{4wt^3}\right) \end{aligned} \tag{1}$$

where F_{mid} is load applied at the mid point of the lap joint, w is the width, t is the thickness of the lap joint an L is the span length. In satrin calculation δ is the displacement value obtained from the center of the

Table 1
The mechanical properties of the aluminum alloys.

Properties	A356	A356-TiB
Elasticity Modulus (GPa)	69.85 ± 2.15	71.35 ± 1.75
Yield Strength (MPa)	82.75 ± 3.75	88.50 ± 4.25
Ultimate Tensile Strength (MPa)	100.5 ± 4.6	118.2 ± 3.15
Failure Strain (%)	2.5 ± 0.25	2.75 ± 0.35

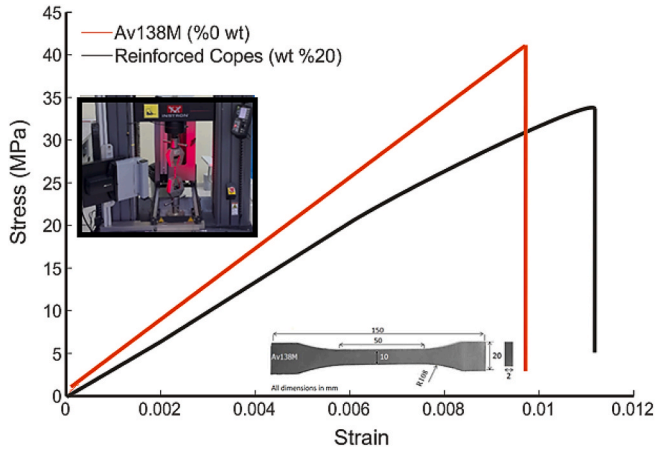

Fig. 3. The stress-strain curves of Av138m.

Table 2
The mechanical properties of the unreinforced and reinforced adhesive.

	Av138M (%0 wt)	Reincorfed Copes (%20)
Elasticity Modulus (MPa)	4204.91	3379.97
Ultimate Tensile Strength (MPa)	37.24	31.90
Failure strain	0.0096	0.0135

lap joint, and m is the slope of the lineer straight line of load displacement curve.

3. Numerical approach

3.1. Finite element analysis of single lap joint

This section indicates the finite element modeling of a single-lap joint using experimental boundary conditions. The purpose of this section is to validate the experimental data by comparing it with the finite element results. In the finite element analysis, the metal and composite adherend making the single-lap joint were modeled using an eight-node solid element, while the adhesive was modeled with a six-node pentahedral cohesive element. Each node of the eight-node elements used to model the composite and metal adherend has a total of six degrees of freedom, which include axial and rotational motions. In this work, a 6-node pentahedral cohesive element was utilized, which provides a new methodology for modeling adhesives in FEA. The cohesive element to model the adhesive layer has six degrees of freedom at each node. The proposed finite element model possesses extra intermediate nodes that carry rotational degree of freedom as opposed to the traditional 8-node solid elements. Secondly, large rotations are expected to take place in the cohesive element due to flexure loading. Large rotations, in general, lead to very severe geometric distortions in the conventional cohesive elements. For these reasons, in the present study, a 6-node pentahedral cohesive element has been proposed, offering enhanced stability and adaptability in transition zones between different mesh types.

3.2. A mixed mode traction separation cohesive zone law

A mixed-mode traction separation law was used in the numerical modeling of the adhesive. The traction-separation law describes the fracture behavior in the cohesive zone model, where the fracture process zone is represented as a single cohesive layer. This framework defines the fracture energies as the maximum energy required for the initiation and propagation of cracks, as specified by the cohesive law. Additionally, the method includes both traction and displacement components in both the normal and shear directions to ensure a comprehensive understanding of the fracture mechanics involved. In the traction separation law, traction stress is expressed as follows [25].

$$T = \frac{T}{\Delta}\left(\beta^2 \Delta_t + \Delta_n\right)\ \mathrm{T} = \frac{\mathrm{T}}{\Delta}\left(\beta^2 \Delta_\mathrm{t} + \Delta_\mathrm{n}\right) \tag{2}$$

where Δ cohesive displacement and the subscripts t and n indicate the tangential and normal displacements, respectively. β is the mixed mode parameter. Cohesive failure occurs under loading when traction stresses peak (T_{nmax}, T_{tmax}) and reach their corresponding cohesive displacements ($\Delta_{n\ max}$ Δ_{tmax}).The strain energy release rate for both mode I and mode II can be written based on these values [25]

$$G_{IC} = \frac{T_{nmax}\Delta_{nmax}}{2}\quad G_{IIC} = \frac{T_{tmax}\Delta_{tmax}}{2} \tag{3}$$

It should be stated here that the expressions utilized to define the traction separation cohesive zone model, along with the corresponding equations provided above, are implemented using the values outlined in Table 3 in the finite element analysis.

3.3. Implementation of the finite element analysis

The numerical model was generated using the explicit finite element software LS-DYNA. The first step in that direction was the generation of

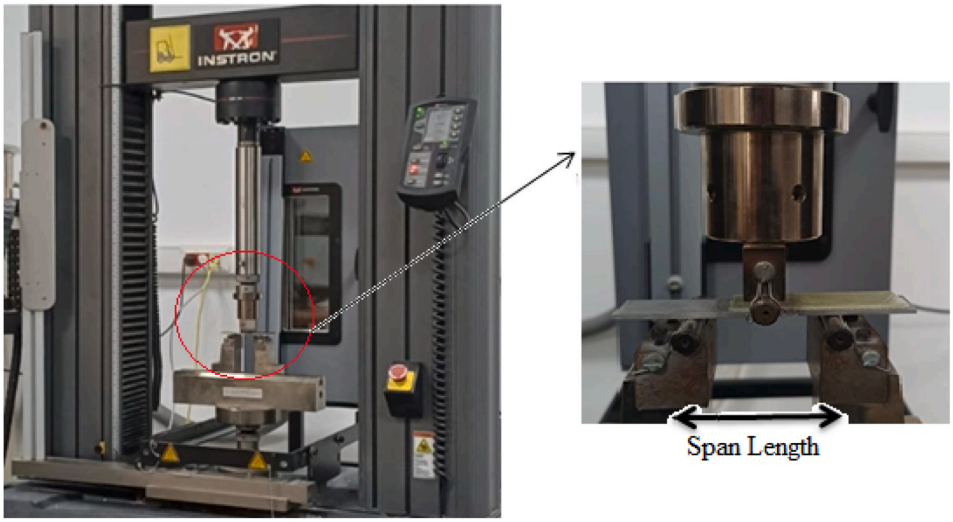

Fig. 4. The three-point flexural test set up.

Table 3
The cohesive parameters for the adhesive [26,27].

	Av138M
Strain energy release rate(mode I) (N/mm)	0.2
Strain energy release rate (mode II) (N/mm)	0.38
Traction in normal direction (MPa)	39.5
Traction in tangential direction (MPa)	30
Young's modulus, E (GPa)	4.89
Poisson's ratio	0.35

geometry corresponding to the experimental setup. An orthotropic material model was assigned to the composite components, while an isotropic elastic material model was allocated to the metallic adherends. Solid elements were employed to model the adherends of the single-lap joint, while the adhesive layer was modeled using the mixed-mode cohesive material model (MAT 138) available in LS-DYNA. During implementation of boundary conditions, the supports in contact with the single lap joint are constrained in translation along the z-direction, while rotations are unconstrained in all directions. In contrast, the impactor that will inflict the bending load is only free to translate along the z-direction, while its motion in all rotations is constrained. Therefore, the impactor was modeled at the midpoint of the overlap region using a two-way surface-to-surface contact element. Because of the complicated nature of deformation under flexure loading, it is very difficult to predict the damage orientation of the interacting parts with high accuracy. Thus, the two-way contact formulation is deemed as the most appropriate solution to capture the mentioned interaction [28]. Another similar contact element was created between adherends and supports, and a definition of master and slave surfaces was done to reduce the amount of penetration. Designation of the master surface was given to the cylindrical surfaces which will transfer the load, while the surface which receives the load was referred to as the slave surface. To maintain mesh sensitivity, the cohesive layer was discretized into 5616 nodes and 3550 elements, while the adherends consisted of 1875 nodes and 2750 elements, as depicted in Fig. 5.

4. Multi-criteria decision making (Grey Relation analysis)

In the GRA model, it is a prerequisite to cumulatively consider the judgment of different evaluators about the relative weights of different criteria. This relative weight has prime importance, as it acts like a multiplier in the GRA model [29]. Being a complex problem, determining the appropriate design of a metal-composite lap joint requires multiple interacting criteria. The multi-criteria decision-making (MCDM) technique used here, therefore, is the GRA method. MCDM techniques permit the treatment of experimental data under a comparable framework. GRA works on the basis of pairwise comparisons of criteria and thus allows detailed performance ranking to help select the best design.

4.1. Analytical Hierarchy Process (AHP)

In the Analytical Hierarchy Process (AHP) method, the first step in determining criteria weights is to create a hierarchical structure. This hierarchical structure is essential for the decision-making process, allowing for a systematic analysis of the problem. It organizes the decision-making issue into layers, starting from the overall objective and descending through the criteria and alternatives at lower levels.

The second part of the AHP (Analytic Hierarchy Process) involves creating a pairwise comparison matrix. In this step, the criteria are compared against each other based on the judgments of the decision-makers. During this comparison process, the subjective judgments of the decision-makers are quantified using numerical values. The degree of preference in the pairwise comparisons, as shown in Table 4, indicates the intensity of importance assigned to each criterion. A five-level rating scale was used, which includes the categories: essential, extremely important, very important, moderately important, and somewhat important [29]. This scale helps to determine the priority weights of the criteria through pairwise evaluation.

A comparison matrix, referred to as matrix A, is developed based on the values derived from experimental results concerning the pairwise

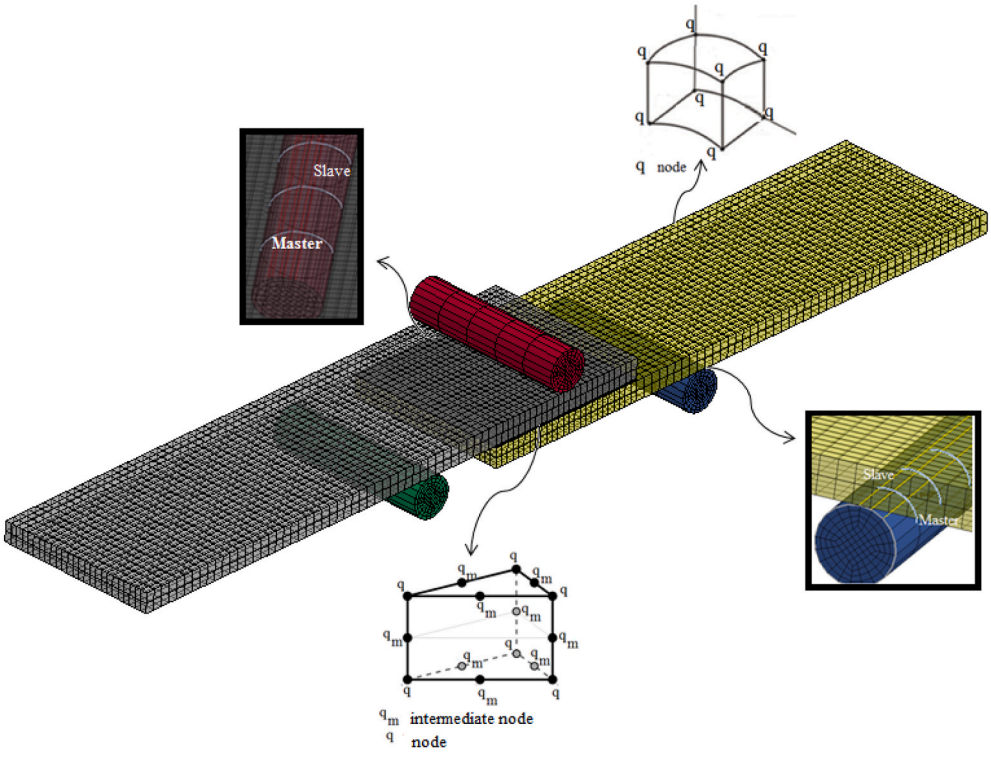

Fig. 5. Finite element model of single lap joint.

Table 4
Saaty (1–9) preference scale [30].

Defination	Scale Value
Equal Important	1
Weakly Important	3
Strongly Important	5
Very Strongly Important	7
Extremely Important	9
Intermediate values between adjacent scales	2,4,6,8

comparisons of criteria. When evaluating a decision problem with respect to n criteria, the pairwise comparison of criterion i with criterion j generates a square matrix of order n × n. Each entry, a_{ij}, within matrix A reflects the comparative value of criterion i in relation to criterion j. In this matrix, the value of a_{ij} is equal to 1 if and only if i is equal to j, while a_{ji} is defined as $1/a_{ij}$

$$A=\begin{bmatrix} 1 & a_{12} & \dots & a_{1n} \\ 1/a_{12} & 1 & \dots & a_{2n} \\ . & & & . \\ . & & & . \\ . & & & . \\ 1/a_{1n} & 1/a_{2n} & \dots & 1 \end{bmatrix}$$

The third step in the Analytical Hierarchy Process (AHP) involves the normalization of the comparison matrix that evaluates the criteria in pairs. This procedure utilizes equation (4) to generate the normalized matrix.

$$c_{ij}=\frac{a_{ij}}{\sum_{j=1}^{n} c_{ij}} \tag{4}$$

The criteria weights for each criterion are found using equation (5).

$$w_i=\frac{1}{n}\sum_{j=1}^{n} c_{ij} \tag{5}$$

The final step of the AHP process is to conduct the consistency test. Comparisons are often influenced by subjective judgments, which can lead to some inconsistencies. To maintain consistency in these judgments, the consistency of pairwise comparisons is assessed using the consistency ratio (CR). The consistency ratio is determined by dividing the consistency index (CI) by the random index (RI) corresponding to matrices of the same rank. [31]. To calculate the CI index, first multiply the pairwise comparison matrix by the criterion weight matrix to determine the priority vector.

$$V=\begin{bmatrix} 1 & a_{12} & \dots & a_{1n} \\ 1/a_{12} & 1 & \dots & a_{2n} \\ . & & & . \\ . & & & . \\ . & & & . \\ 1/a_{1n} & 1/a_{2n} & \dots & 1 \end{bmatrix} * \begin{bmatrix} w_1 \\ w_2 \\ . \\ . \\ . \\ . \\ w_n \end{bmatrix}$$

Subsequently, the eigenvector is calculated using $\lambda_i = \frac{v_i}{w_i}$, and the priority vector is determined using the $\lambda_{max} = \frac{\sum_{i=1}^{n} \lambda_i}{n}$ equation. Then, the consistency index (CI) is calculated using the following equation;

$$CI=\frac{\lambda_{max-n}}{n-1} \tag{6}$$

The random inconsistency index (RI) value is dependent on the number of criteria (n), which can be found in Table 5 [32].

Following the calculation of the CI and RI values, the consistency index can be accurately determined by applying equation 7

$$CR=\frac{CI}{RI} \tag{7}$$

A CR value below 0.1 indicates that judgments are fairly consistent. In such cases, the calculated weights can be used as the final criterion weights in the analysis.

4.2. Grey relation analysis (GRA)

The Grey Relationship Analysis (GRA) method is used multi-criteria decision-making technique for analyzing relationships in multi-criteria environments. Its primary purpose is to identify the fundamental relationships between factors and alternatives [30]. In the decision-making process, a decision matrix is created, where the alternatives (i = 1, 2, …, m) are represented as rows and the criteria (j = 1, 2, …, n) are represented as columns. This matrix displays the performance values of each alternative across each criterion. The decision matrix was constructed based on the comparability sequences as outlined below

$$X=\begin{bmatrix} x_1(1) & \cdots & x_1(n) \\ \vdots & \ddots & \vdots \\ x_m(1) & \cdots & x_m(n) \end{bmatrix}$$

where, $x_i(j)$ shows the performance of the ith alternative against the jth criterion. Furthermore,the $x_0(j)$ expression in the $x_0 = (x_0(j))$ equation used to determine the reference sequence represents the best value of the j criterion among the values. Using decision matrix X and the equations in 8-9, the normalized decision matrix is expressed as follows

$$x_i(j)=\frac{x_i(j)-min_j x_i(j)}{max_j x_i(j)-min_j x_i(j)} \quad \textit{for benefit criteria} \tag{8}$$

$$x_i(j)=\frac{max_j x_i(j)-x_i(j)}{max_j x_i(j)-min_j x_i(j)} \quad \textit{for cost criteria} \tag{9}$$

$$X^*=\begin{bmatrix} x_1^*(1) & \cdots & x_1^*(n) \\ \vdots & \ddots & \vdots \\ x_m^*(1) & \cdots & x_m^*(n) \end{bmatrix}$$

where, X^* is the normalized decision matrix.

After determining the normalized matrix, an Absolute Value is created. The $\Delta_{0i}(j)$ matrix is created by calculating the distance between the reference series and the normalized values using equation (10).

$$\Delta_{0i}(j)=\left|x_0^*(j)-x_i^*(j)\right| \tag{10}$$

$$\Delta_{0i}(j)=\begin{bmatrix} \Delta_{01}(1) & \cdots & \Delta_{01}(n) \\ \vdots & \ddots & \vdots \\ \Delta_{0m}(1) & \cdots & \Delta_{0m}(n) \end{bmatrix}$$

The next step in the GRA process is to determine the Grey Relational Coefficient (GRC). GRC quantifies the relationship between the reference sequence and each comparable sequence. This coefficient is calculated using normalized data, following the expression below [33].

$$\gamma_{0i}(j)=\frac{\Delta_{min}+\zeta\,\Delta_{max}}{\Delta_{oi}(j)+\zeta\,\Delta_{max}} \tag{11}$$

The distinguishing coefficient ζ is commonly set at 0.5. It adjusts the sensitivity of the grey relationship coefficients, taking values between 0 and 1.

In the final step of the GRA process, a grey relational score is calculated to measure the degree of similarity between the comparable sequence and the reference sequence. A higher grey relational score indicates a better alternative, while a lower score signifies a worse alternative.

$$\Gamma_{0i}=\sum_{j=1}^{n} w_j(j)\gamma_{0i}(j) \tag{12}$$

where, Γ_{0i} is the grey relational score.

Table 5
The value of Random Consistency Index [32].

N	1	2	3	4	5	6	7	8	9	10
RI	0	0	0.5799	0.8921	1.1159	1.2358	1.3322	1.3952	1.4537	1.4882

5. Results and Discussion

5.1. Experimental results

The load-displacement curves for metal composite lap joints, evaluated under various flexural loading rates, are presented in Figs. 6–8. The data indicate that, across all loading rates, the maximum bending capacity of the lap joints increases with an increase in rate. Notably, lap joints constructed with thermoplastic-reinforced adhesives demonstrated lower flexural loads and higher displacements at each loading rate when compared to those made with neat adhesives. Fig. 3 shows that adding thermoplastic reinforcement to the adhesive enhances ductility. This behavior is also observed in the metal composite lap joint, as illustrated in Figs. 6–8. It can be concluded that the co-polyester thermoplastic (Copes) reinforcement employed in this study effectively enhances the ductility of the metal-composite lap joints.

The load-displacement curves obtained for all rates were employed to calculate the flexural modulus and absorbed energy of the lap joints. The flexural modulus was calculated using the load-displacement curve data from the interface of the universal testing machine. Additionally, the values for absorbed energy were determined by calculating the area under the load-displacement curve. The experimental results are provided in Table 6.

It has been made clear in Table 6 that as the loading rate increases, the forces in single lap joints tend to rise. This improvement in force is traced to the viscoelastic property of epoxy adhesive, causing it to behave elastically to a greater extent and behave plastically to a lesser extent as the loading rate increases. Therefore, epoxy adhesive is particularly sensitive to changes in loading rates [34]. However, in lap joints constructed with co-polyester-reinforced adhesive, the flexural modulus was observed to be lower than that of lap joints made with neat adhesive, whereas the absorbed energy values were higher. Furthermore, in thermoplastic-reinforced metal composite joints, the incorporation of thermoplastic reinforcement resulted in a decrease in maximum bending strength while simultaneously enhancing the absorbed energy values at all rates. The incorporation of thermoplastic reinforcement in metal composite lap joints significantly enhances their capacity to absorb energy. It can be said that this improvement results in a delayed initiation of cracks and a reduction in crack propagation, thereby increasing the overall resistance to fracture damage [35].

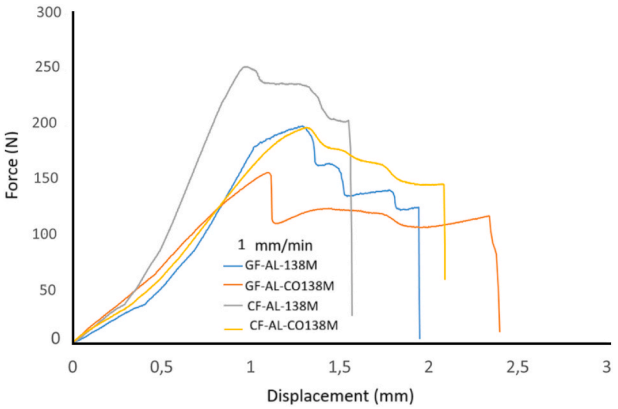

Fig. 6. Load –displacement curves of lap joint under 1 mm loading rate.

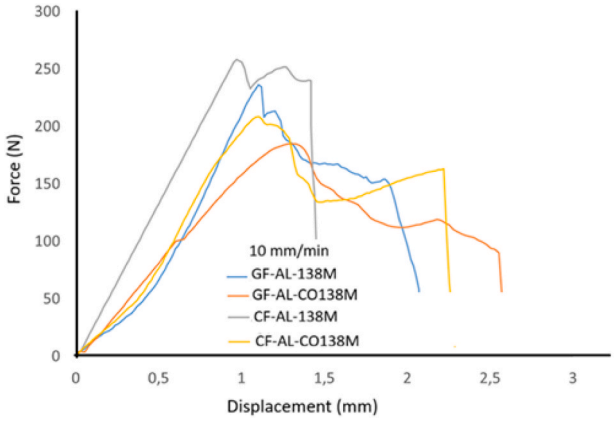

Fig. 7. Load –displacement curves of lap joint under 10 mm loading rate.

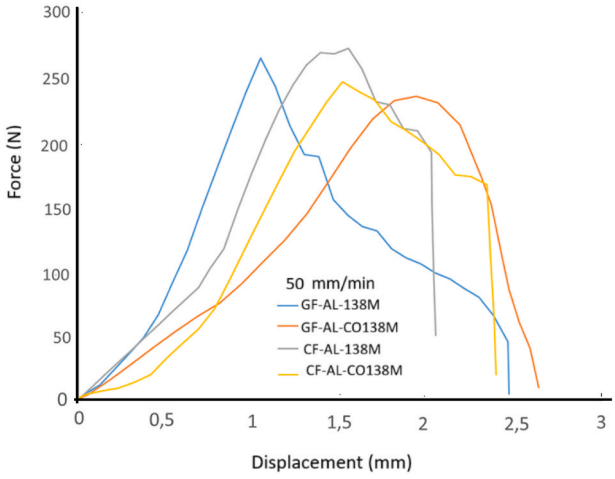

Fig. 8. Load –displacement curves of lap joint under 50 mm loading rate.

5.2. Numerical results

In this section, the results obtained from the experimental approach are compared with those obtained from numerical analysis to verify the experimental results. Additionally, we examine the deformations observed in the experimental tests alongside the deformation images obtained from the numerical analysis. Fig. 9 indicates a comparison of the deformation images of the metal composite lap joint after flexural load, utilizing the experimental and numerical approaches.

Fig. 9 shows three images each that highlight the behavior of the metal composite lap joint under flexural loading and its development until failure. The first image represents the initial state of the lap joint under bending load. The second image shows the crack formation inside the lap joint due to the increase in flexural deformation. Then, the third image points out that these cracks grow with the increase in flexural load and deformation, which resulted in complete separation. All the deformations observed within the experimental approach also occurred in the numerical analysis, as shown in Fig. 9. Furthermore, the image in the figure depicts the GF-Al-138M joint at a rate of 1 mm/min. For the sake of brevity, it is not possible to depict the experimental numerical

Table 6
The experimental results for all metal composite joints.

Lap joint	Maximum Force (N)	Failure displacement (mm)	Flexural Modulus (MPa)	Absorbed Energy (Nmm)
GF-AL-138M-1 mm/min	195.32 ± 12.48	1.95 ± 0.22	9976 ± 355	212.18 ± 13
GF-AL-CO138M-1mm/min	153.30 ± 14.99	2.39 ± 0.18	6183 ± 250	232.30 ± 12
CF-AL-138M-1 mm/min	248.36 ± 15.02	1.57 ± 0.2	11420 ± 375	233.95 ± 17.2
CF-AL-CO138M-1mm/min	190.26 ± 11.34	2.09 ± 0.26	7525 ± 409	249.43 ± 14.6
GF-AL-138M-10 mm/min	234.42 ± 19.88	2.08 ± 0.16	10847 ± 369	262.41 ± 18.2
GF-AL-CO138M-10 mm/min	184.73 ± 15	2.6 ± 0.25	7578 ± 289	290.38 ± 16.8
CF-AL-138M-10 mm/min	257.2 ± 20.42	1.46 ± 0.19	12679 ± 505	249.83 ± 13.5
CF-AL-CO138M-10 mm/min	208.3 ± 17.36	2.28 ± 0.15	7932 ± 303	288.84 ± 15.6
GF-AL-138M-50 mm/min	261.957 ± 14.83	2.46 ± 0.21	11937 ± 488	298.95 ± 17.89
GF-AL-CO138M-50 mm/min	232.86 ± 23.43	2.63 ± 0.24	8334 ± 296	317.58 ± 10.88
CF-AL-138M-50 mm/min	269.34 ± 16.36	2.04 ± 0.12	13282 ± 412	310.07 ± 14
CF-AL-CO138M-50 mm/min	243.76 ± 21.67	2.16 ± 0.16	8568 ± 366	312.64 ± 12.6

± Standard deviation.

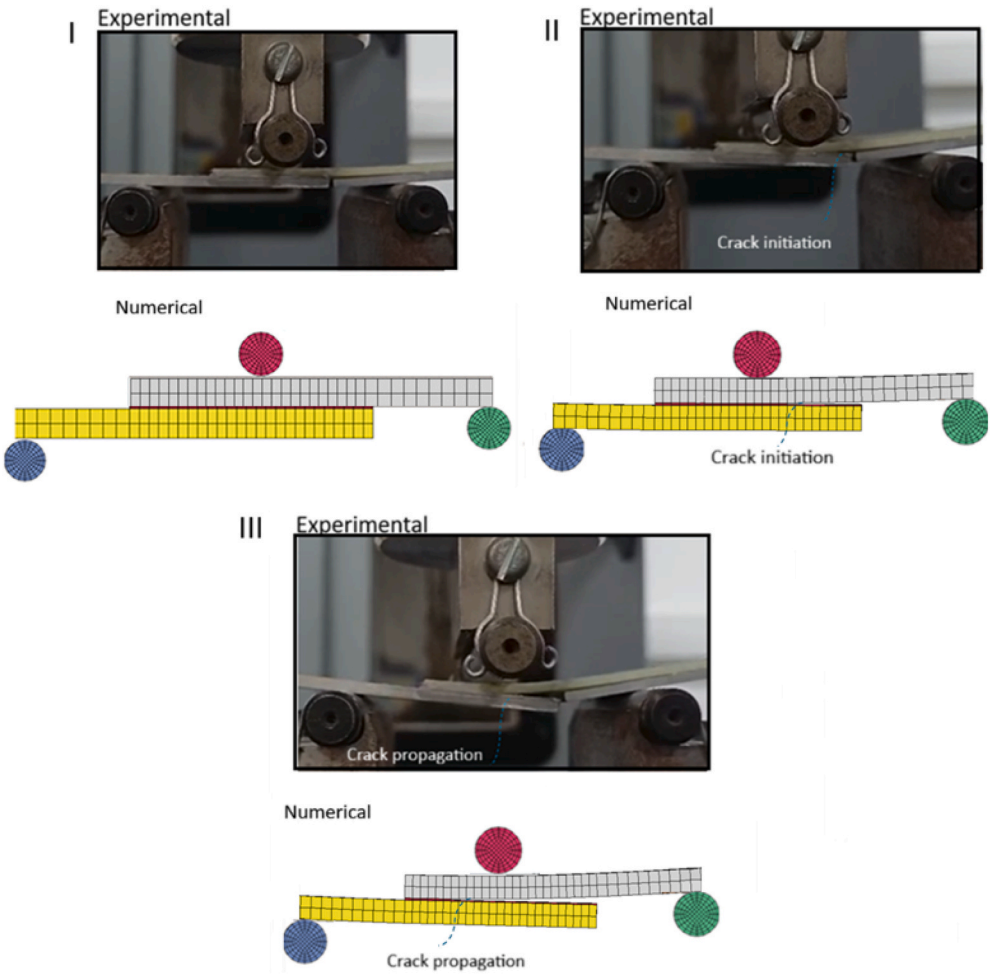

Fig. 9. Comparison of the deformation images of lap joints for experimental and numerical approaches.

deformation images of all lap joints and of all loading rates tested in this work. However, similar deformation was obtained from all experiments and numerical approaches.

The applied load is transferred to the adhesive through the lap joints, and cohesive damage is observed on the adherend surface. This observation proves that the lap joint was created correctly. In this study, cohesive damage was observed on both composite and metal surfaces at all loading rates. Furthermore, it is also seen that the cohesive damage regions change as the loading rate changes. Fig. 10 presents the cohesive damage in both types of lap joints under the rate of 10 mm/min. Additionally, numerical analysis showed cohesive damage in the adherends, which was in very good agreement with the experimental tests. The cohesive damage determined with the numerical approach is a key parameter showing that the cohesive element used in this study was correct. It is well known that rotational deformations of the lap joint occurring at bending loads cause geometric distortions of the cohesive element. Such distortions are difficult to model using the conventional eight-node cohesive element. However, the methodological approach using the improved cohesive element with intermediate nodes applied in this study allows for large deformations in the cohesive element to be detected [36]. Cohesive damage results of the numerical model validate this approach more.

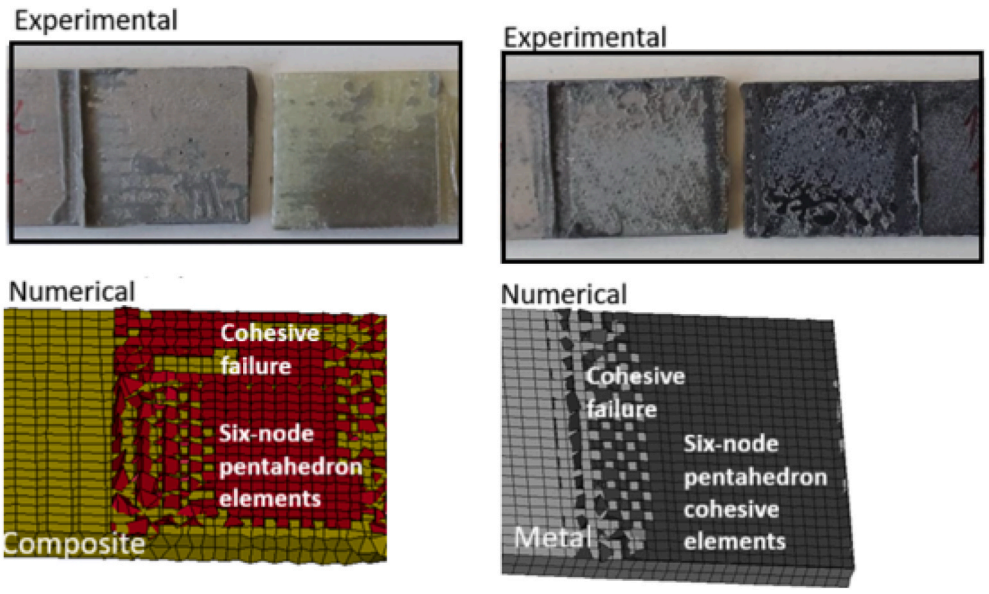

Fig. 10. Cohesive damage representation in experimental and numerical approach.

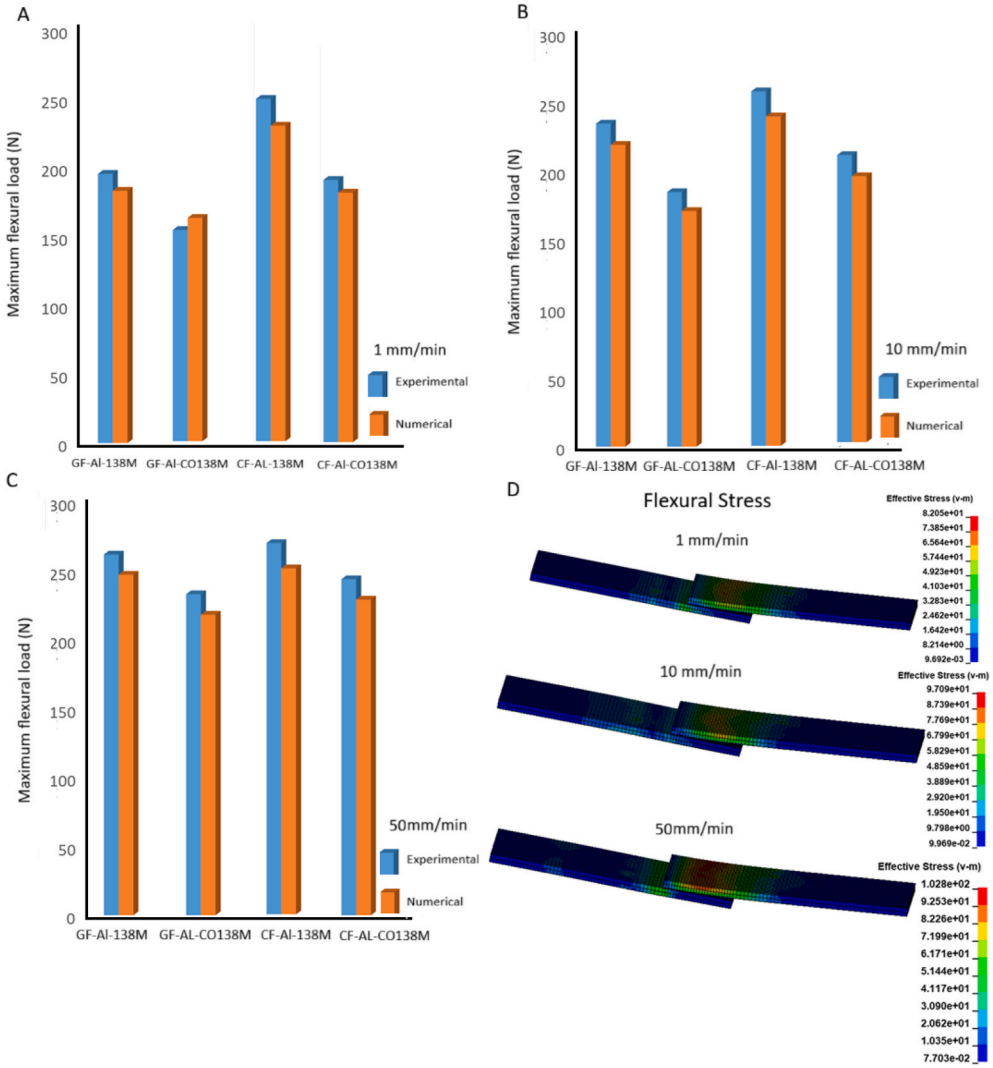

Fig. 11. Comparison of maximum loads obtained by experimental and numerical approach.

The maximum load and damage displacement values obtained through the experimental approach have been compared with those derived from the numerical approach, as presented in Figs. 11 and 12. Furthermore, the flexural stress and strain results for various rates within the numerical model are also detailed in these figures (refer to Section D).

Figs. 11 and 12 demonstrate that the maximum load and failure displacement values obtained from the experimental approach align closely with those from the numerical approach. The highest difference in maximum load values between the experimental and numerical methods across different rates was found to be approximately 7 percent, while the lowest differences were around 4 percent. For failure displacement, the highest error recorded was about 8 percent, and the lowest was approximately 5 percent. Furthermore, as illustrated in Fig. 11, the maximum flexural stress for the GF-AL-138M lap joint, calculated at three different rates using the numerical approach, exhibits correlation with the flexural stresses obtained through the experimental method, following the equation presented in Equation (1) for the relevant maximum load values. Correspondingly, the strain values derived from the numerical model for the same lap joint are consistent with those calculated using Equation (1) across all tested rates. In summary, the assessment of the deformation of the lap joint under flexural load, the cohesive damage observed on the adherends, and the convergence of the maximum load-displacement values collectively affirm that the experimental results are substantiated by the numerical analysis.

5.3. GRA result

In this study, the GRA approach was applied to determine the most suitable metal-composite lap joint design that would provide the highest flexural performance under various loading rates. The performance criteria to be considered in the decision-making process were defined as Maximum Force (N), Failure Displacement (mm), Flexural Modulus (MPa), and Absorbed Energy (Nmm), and the relative importance of these criteria was determined using the Analytical Hierarchy Process (AHP) method. Based on the obtained criteria weights, 12 different metal-composite joint alternatives were evaluated in the second stage, and their performance rankings were determined. To assess the optimum flexural performance of various metal-composite lap joints, a decision matrix was developed, consisting of twelve alternative designs and four performance criteria (See Table 6). In this (12 × 4) matrix, the rows represent the alternative designs, while the columns correspond to the performance criteria. The matrix includes the experimental results for each alternative, measured against each criterion. To determine the weights of the criteria, the analysis result of the flexural behavior of single lap joints was considered based on the literature [37,38]. Pairwise comparisons among the criteria were carried out using Table 7.

The normalization process was conducted in accordance with Equation (4), and the resultant normalized matrix of the criteria is summarized in Table 8.

After obtaining the normalized decision matrix. the weight values for each criterion were calculated using Equation (5). The weights determined from this process indicate the importance of each criterion in the decision-making process. According to the Analytic Hierarchy Process (AHP) method. the Maximum Force criterion was identified as the most important. To ensure the reliability of the resulting weights. a consistency analysis was performed. In this analysis. we first calculated the priority vector (V) and the maximum Eigenvalue (λ_{max}).

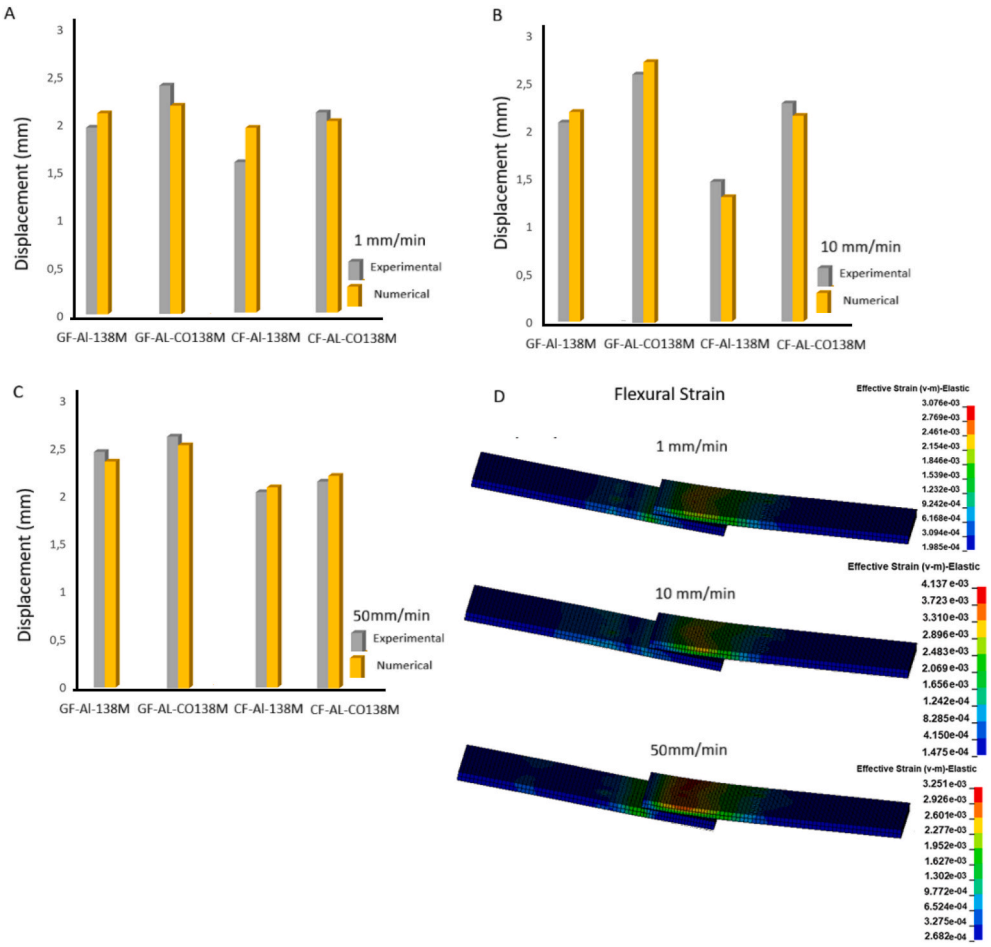

Fig. 12. Comparison of displacements obtained by experimental and numerical approach.

Table 7
Pairwise comparisons.

Criteria	Maximum Force (N)	Failure displacement (mm)	Flexural Modulus (MPa)	Absorbed Energy (Nmm)
Maximum Force (N)	1	9	7	6
Failure displacement (mm)	1/9	1	1/6	1/5
Flexural Modulus (MPa)	1/7	6	1	1
Absorbed Energy (Nmm)	1/6	5	1	1

$$V=\begin{bmatrix} 1 & 9 & 7 & 6 \\ \frac{1}{9} & 1 & \frac{1}{6} & \frac{1}{5} \\ \frac{1}{7} & 6 & 1 & 1 \\ \frac{1}{6} & 5 & 1 & 1 \end{bmatrix} * \begin{bmatrix} 0.656956 \\ 0.042101 \\ 0.154329 \\ 0.146614 \end{bmatrix} = \begin{bmatrix} 2.995849 \\ 0.17014 \\ 0.647399 \\ 0.62094 \end{bmatrix}$$

$$\lambda_i = \begin{bmatrix} 2.995849 \\ 0.17014 \\ 0.647399 \\ 0.62094 \end{bmatrix} \Big/ \begin{bmatrix} 0.656956 \\ 0.042101 \\ 0.154329 \\ 0.146614 \end{bmatrix} = \begin{bmatrix} 4.560195 \\ 4.041255 \\ 4.194932 \\ 4.235202 \end{bmatrix} \rightarrow \lambda_{max} = 4.257896$$

The consistency index (CI) was calculated using Equation (6). For a sample size of n = 4. the random inconsistency index (RI) was taken to be 0.89. In the final step the consistency ratio (CR) was determined by comparing the obtained consistency index (CI) value with the random inconsistency index (RI). Since the CR value of 0.09659 was less than 0.1. the comparisons were deemed consistent. The significance levels of the four criteria evaluated in the study using AHP analysis (*Maximum Force*. *Failure Displacement*. *Flexural Modulus*. *and Absorbed Energy*) were determined to be 0.656956. 0.042101. 0.154329. and 0.146614. respectively.

Since all the criteria were of the benefit type the decision matrix was normalized using Equation (8). In this process each criterion value was adjusted to fall within the [0. 1] range by considering the minimum and maximum values in its respective column. This normalization ensured that all criteria were on the same scale making them comparable.

Following the identification of the reference sequence (see Table 9) the Grey Relational Coefficient is calculated using Equation (10) through (11), Subsequently the Grey Relational Grade is determined using Equation (12). The alternatives are then ranked accordingly and the final results along with the rankings are presented in the summary below.

Based on the ranking from the GRA analysis presented in Table 10, the most favorable flexural behavior across various loading rates was observed for the CF-AL-138M lap joint at a rate of 50 mm/min. In contrast, the GF-AL-CO138M lap joint exhibited the least favorable flexural behavior at a loading rate of 1 mm/min.

6. Conclusion

This research focused on optimizing the flexural behavior of a metal-composite lap joint bonded with a co-polyester-reinforced epoxy adhesive across various loading rates. Three-point flexural tests at multiple loading rates were carried out in order to assess the flexural performance of the joint. In the numerical investigation, a 6-node pentahedral cohesive element, which introduces a new approach for simulating adhesive layers within finite element analysis, was utilized. We then compared experimental data with the ones obtained from the finite element simulations to validate the results. Finally, the optimal flexural performance of the metal-composite joints under different loading rates through the use of the Grey Relational Analysis was determined. The results obtained can be explained as follows:

- The maximum bending capacity of the lap joints was found to increase with the increase in loading rate across all loading rates. Again, it was revealed that thermoplastic-reinforced adhesives used to form lap joints exhibit lower flexural loads at all loading rates but higher displacements compared to those bonded by neat adhesives. These results confirm that the thermoplastic co-polyester reinforcement employed in this work enhances the ductility of metal–composite lap joints accordingly. It was also noticed that

Table 9
Reference sequences of the criteria in the GRA process.

Lap joint	Maximum Force (N)	Failure displacement (mm)	Flexural Modulus (MPa)	Absorbed Energy (Nmm)
GF-AL-138M-1 mm/min	0.3621	0.4188	0.5343	0.0000
GF-AL-CO138M-1mm/min	0.0000	0.7949	0.0000	0.1909
CF-AL-138M-1 mm/min	0.8192	0.0940	0.7377	0.2065
CF-AL-CO138M-1mm/min	0.3185	0.5385	0.1890	0.3534
GF-AL-138M-10 mm/min	0.6991	0.5299	0.6570	0.4766
GF-AL-CO138M-10 mm/min	0.2709	0.9744	0.1965	0.7419
CF-AL-138M-10 mm/min	0.8954	0.0000	0.9151	0.3572
CF-AL-CO138M-10 mm/min	0.4740	0.7009	0.2464	0.7273
GF-AL-138M-50 mm/min	0.9364	0.8547	0.8105	0.8232
GF-AL-CO138M-50 mm/min	0.6856	1.0000	0.3030	1.0000
CF-AL-138M-50 mm/min	1.0000	0.4957	1.0000	0.9287
CF-AL-CO138M-50 mm/min	0.7796	0.5983	0.3360	0.9531
Reference Sequence $x_0(j)$	**1.0000**	**1.0000**	**1.0000**	**1.0000**

Table 8
Normalize matrix of the criteria.

Criteria	Maximum Force (N)	Failure displacement (mm)	Flexural Modulus (MPa)	Absorbed Energy (Nmm)	Criterion Weights
Maximum Force (N)	0.703911	0.428571	0.763636	0.731707317	0.656956
Failure displacement (mm)	0.078212	0.047619	0.018182	0.024390244	0.042101
Flexural Modulus (MPa)	0.100559	0.285714	0.109091	0.12195122	0.154329
Absorbed Energy (Nmm)	0.117318	0.238095	0.109091	0.12195122	0.146614

Table 10
Grey relational grade and the ranking order of the lap joints.

Criterion Weights w_i	0.656956	0.042101	0.154329	0.146614	Grey relational grade	
Lap joint	Maximum Force (N)	Failure displacement (mm)	Flexural Modulus (MPa)	Absorbed Energy (Nmm)		Ranking
GF-AL-138M-1 mm/min	0.43941	0.46245	0.51776	0.33333	0.436921	10
GF-AL-CO138M-1mm/min	0.33333	0.70909	0.33333	0.38194	0.356279	12
CF-AL-138M-1 mm/min	0.73443	0.35562	0.65592	0.38656	0.655363	6
CF-AL-CO138M-1mm/min	0.42319	0.52000	0.38140	0.43608	0.422709	11
GF-AL-138M-10 mm/min	0.62427	0.51542	0.59312	0.48855	0.594983	7
GF-AL-CO138M-10 mm/min	0.40679	0.95122	0.38358	0.65957	0.463189	9
CF-AL-138M-10 mm/min	0.82697	0.33333	0.85479	0.43753	0.75338	3
CF-AL-CO138M-10 mm/min	0.48732	0.62567	0.39884	0.64710	0.502915	8
GF-AL-138M-50 mm/min	0.88712	0.77483	0.72520	0.73882	0.835658	2
GF-AL-CO138M-50 mm/min	0.61397	1.00000	0.41771	1.00000	0.65653	5
CF-AL-138M-50 mm/min	1.00000	0.49787	1.00000	0.87527	0.960573	1
CF-AL-CO138M-50 mm/min	0.69402	0.55450	0.42954	0.91430	0.679624	4

thermoplastic reinforcement in the metal composite lap joints greatly improves their energy-absorbing capacity. Localized delay in crack onset and reduced crack propagations due to such reinforcement increase the resistance to fracture damage.

- Numerical results provide the deformation in the lap joint under the bending load cohesive damage on the adherends, and the load-displacement values for the maximum load, which is close to experimental results; this is proof of the validity of the experimental data. Moreover, it should be noticed that the identified cohesive damage in the numerical approach is an important factor that indicates the accuracy of the used cohesive element in this study. The rotational deformations in the lap joint due to flexural loads involve geometric distortions in the cohesive element, which can hardly be accounted for with the use of a traditional eight-node cohesive element. However, this study is performed with an enhanced cohesive element with intermediate nodes, allowing the identification of notable deformations within the cohesive element.
- The GRA method was used to evaluate and rank the performance of metal-composite joints to identify the best configuration. The ranking in Table 10 shows that CF-AL-138M gave the best flexural performance for a loading rate of 50 mm/min, while the worst result of flexural performance, at 1 mm/min loading rate corresponded to the GF-AL-CO138M lap joint configuration.

CRediT authorship contribution statement

Engin Erbayrak: Writing – original draft, Methodology, Conceptualization. **Seda Erbayrak:** Writing – original draft, Software, Investigation. **Beril Eker:** Validation, Methodology, Formal analysis. **Murat Colak:** Writing – review & editing, Methodology, Investigation.

Declaration of competing interest

The authors declare that they have no known competing financial interests or personal relationships that could have appeared to influence the work reported in this paper.

Data availability

The authors do not have permission to share data.

References

[1] Pittaa S, Carlesb VM, Rourec F, Crespod D, Rojasa JI. On the static strength of aluminium and carbon fibre aircraft lap joint repairs. Compos Struct 2018;201:276–90. https://doi.org/10.1016/j.compstruct.2018.06.002.

[2] Ekladious A, Wang J, Chowdhury N, Chiu WK. Mechanical performance of hybrid double- and step-lap joints in primary metallic aircraft structures: an experimental and numerical approach. Compos Part C 2025;16:100554. https://doi.org/10.1016/j.jcomc.2024.100554.

[3] Kupski J, Freitas ST. Design of adhesively bonded lap joints with laminated CFRP adherends:Review, challenges and new opportunities for aerospace structures. Compos Struct 2021;268:113923. https://doi.org/10.1016/j.compstruct.2021.113923.

[4] Rezvaninasab M, Farhadinia M, Mirzaei A, Ramzaninezhad M, Khamseh F, Alaei Mh. Experimental evaluation of reinforcing the single lap joint in both longitudinal and transverse direction under tensile and bending condition. Int J Adhesion Adhes 2019;88:19–25. https://doi.org/10.1016/j.ijadhadh.2018.05.020.

[5] Darla VR, Ben BS, Srinadh KVS. Evaluation of strength and performance for a single lap bonded joint by insertion of structural elements in adhesive. Int J Adhesion Adhes 2022;118:103240. https://doi.org/10.1016/j.ijadhadh.2022.103240.

[6] Esmaeili E, Razavi N, Bayat M, Berto F. Flexural behavior of metallic fiber-reinforced adhesively bonded single lap joints. J Adhes 2018;94(6):453–72. https://doi.org/10.1080/00218464.2017.1285235. 2018.

[7] Zeinedini A, Hosseini Y, Mahdi AS, Safar AA, Silva LFM. Impact of the manufacturing process on the flexural properties of laminated composite-metal riveted joints: experimental and numerical studies. Appl Compos Mater 2024;31:583–610. https://doi.org/10.1007/s10443-023-10186-w.

[8] Sadık A, Karabudak F. Strength analysis in bonded, bolted and bolted-bonded joints, single lap joints, metal/composite plates. Appl Sci 2023;103(6):10476. https://doi.org/10.3390/app131810476.

[9] Etri HE, Polat MZ, Kadioglu F. Numerical and experimental 3-point bending quasi-static flexural behavior of single-strap joints joined using AF163-2K adhesive films. J Adhes 2024;100(16):1595–622. https://doi.org/10.1080/00218464.2024.2342338.

[10] Papanicolaou GC, Karagiannis D, Kousiatza C, Kontaxis LC, Portan DV. Flexural behavior of single-lap joints of similar and dissimilar adherends. J Adhes Sci Technol 2023;37:624–48. https://doi.org/10.1080/01694243.2022.2035050.

[11] Kadioglu F, Demiral M. Failure behaviour of the single lap joints of angle plied composites under three point bending test. J Adhes Sci Technol 2020;34:531–48. https://doi.org/10.1080/01694243.2019.1674101.

[12] Azama A, Mubashara A, Ashcroftb IA, Uddina E, Jaffery SHI. A numerical study of the effect of ply-layup on the strength and stiffness of a composite T-joint under three point bending. J Adhes Sci Technol 2017;31:2124–38. https://doi.org/10.1080/01694243.2017.1278818.

[13] Leea C, Leea JW, Ryub SG, Oh JH. Optimum design of a large area, flexure based XYθ mask alignment stage for a 12-inch wafer using grey relation analysis. Robot Comput Integrated Manuf 2019;58:109–19. https://doi.org/10.1016/j.rcim.2019.02.005.

[14] Sabry I, Hewidy AM, Alkhedher M, Mourad AHI. Analysis of variance and grey relational analysis application methods for the selection and optimization problem in 6061-T6 flange friction stir welding process parameters. Int J Lightweight Mater Manuf 2024;7:773–92. https://doi.org/10.1016/j.ijlmm.2024.06.0062588-8404.

[15] Dixit N, Jain PK. Multi-objective strength optimization of fused filament fabricated complex flexible parts using grey relational analysis. Iran J Sci Technol Trans Mech Eng 2023;47:1787–97. https://doi.org/10.1007/s40997-022-00589-8.

[16] Renania HK, Mirsalehi SE. Optimization of FSW lap joining of pure copper using taguchi method and grey relational analysis. Mater Res Express 2019;6:056525. https://doi.org/10.1088/2053-1591/ab021d.

[17] Hua P, Shia ZW, Wanga XX, Lia WD, Zhoua SG, Han X. Strength degradation of adhesively bonded single-lap joints in a cyclic temperature environment using a cohesive zone model. J Adhes 2015;91:587–603. https://doi.org/10.1080/00218464.2014.915754.

[18] Erbayrak E, Colak M, Noberi C. Low-velocity impact analysis of metal-composite joints with grain-refined A356 and reinforced epoxy adhesive using six node pentahedron cohesive elements. J Adhes https://doi.org/10.1080/00218464.2025.2531241.

[19] Ji-hua P, Xiao-long T, Jian-ting HE, De-yin XU. Effect of heat treatment on microstructure and tensile properties of A356 alloys. Trans Nonferrous Met Soc China 2011;21:1950–6. https://doi.org/10.1016/S1003-6326(11)60955-2.

[20] Erbayrak Yuncuoglu EU, Kahraman Y, Gumus BE. An experimental and numerical determination on low-velocity impact response of hybrid composite laminate. Iran J Sci Technol Trans Mech Eng 2020;45:665–81. https://doi.org/10.1007/s40997-020-00402-4.

[21] Venugopal A, Sudhagar PE. Enhancing shear and flexural strength of single lap composite joints with a graphene nanoparticle-reinforced adhesive through a co-curing technique. Polym Compos 2024;45:4202–20. https://doi.org/10.1002/pc.28053.
[22] Pizzi A, Mittal KL. Handbook of adhesive technology. third ed. United Kingdom: Taylor& Francis; 2018.
[23] Ramaswamy K, O'Higgins RM, Corbett MC, McCarthy MA, McCarthy CT. Quasi-static and dynamic performance of novel interlocked hybrid metal-composite joints. Compos Struct 2020;253:112769. https://doi.org/10.1016/j.compstruct.2020.112769.
[24] Avendaño Carbas RJC, Marques EAS, Da Silva LFM, Fernandes AA. Effect of temperature and strain rate on single lap joints with dissimilar lightweight adherends bonded with an acrylic adhesive. Compos Struct 2016;152:34–44. https://doi.org/10.1016/j.compstruct.2016.05.034.
[25] Dooley I, Mangala S, Kale L, Geubelle P. Parallel simulations of dynamic fracture using extrinsic cohesive elements. J Sci Comput 2009;39:144–65. https://doi.org/10.1007/s10915-008-9254-0.
[26] Erbayrak E. Investigations of low-velocity impact behaviour of single-lap joints having dissimilar hybrid composite adherends through cohesive zone model approach. J Adhes Sci Technol 2022;36:545–65. https://doi.org/10.1080/01694243.2021.1970373.
[27] Erbayrak E. Numerical investigation of the mode I/Mode II fracture behavior of the hybrid composite joints with a hybrid bondline. J Eng Res 2023;11:527–36. https://doi.org/10.1016/j.jer.2023.100101.
[28] Livermore Software Technology. LSDYA user manuels, vol. II; May 19, 2014. Avaliable, https://ftp.lstc.com.
[29] Yang C, Chen B. Supplier selection using combined analytical hierarchy process and grey relational analysis. J Manuf Technol Manag 2006;17:926–41. https://doi.org/10.1108/17410380610688241.
[30] Saaty TL, Vargas LG. Models, methods, concepts & applications of the analytic hierarchy process. second ed. Pittsburgh: Springer; 2012.
[31] Velmurugan R, Selvamuthukumar S, Manavalan R. Multi criteria decision making to select the suitable method for the preparation of nanoparticles using an analytical hierarchy process. Pharm Times 2011;66:836–42. https://doi.org/10.1691/ph.2011.1034.
[32] Golden BL, Wang Q. An alternative measure of consistency. In: Golden BL, Wasil A, Harker PT, editors. Analytic hierarchy process: applications and studies. New-York: Springer Verlag; 1990. p. 68–81.
[33] Yıldız N, Tuysuz F. A hybrid multi-criteria decision making approach for strategic retail location investment: application to Turkish food retailing. Soc Econ Plann Sci 2019;68:100619. https://doi.org/10.1016/j.seps.2018.02.006.
[34] Guo L, Liu J, Xia H, Li X, Zhang X, Yang H, Yang Y. Effects of loading rate, temperature, and thickness on the tensile strength of precision adhesive joints. Polym Test 2022;109:107528. https://doi.org/10.1016/j.polymertesting.2022.107528.
[35] Shi S, Liu Z, Lv H, Zhou X, Sun Z, Chen B. The tensile properties of adhesively bonded single lap joints with short kevlar fiber. Int J Adhesion Adhes 2024;134:103794. https://doi.org/10.1016/j.ijadhadh.2024.103794.
[36] Erbayrak E. Exploring the strength analysis of a double lap biadhesive joint using hybrid composite adherend and six-node pentahedron cohesive elements under different loading rates. J Adhes Sci Technol 2025;39:2214–35. https://doi.org/10.1080/01694243.2025.2490263.
[37] Khalili SMR, Shokuhfar A, Hoseini SD, Bidkhori M, Khalili S, Mittal RK. Experimental study of the influence of adhesive reinforcement in lap jointsfor composite structures subjected to mechanical loads. Int J Adhesion Adhes 2008;28:436–44. https://doi.org/10.1016/j.ijadhadh.2008.04.009.
[38] Atahan MG, Apalak MK. Loading-rate effect on tensile and bending strength of 3D-printed polylactic acid adhesively bonded joints. J Adhes Sci Technol 2022;36:317–44. https://doi.org/10.1080/01694243.2021.1922022.